Double Mutation at the Subunit Interface of Glutathione Transferase rGSTM1-1 Results in a Stable, Folded Monomer†

Lawrence C. Thompson,‡ John Walters,§ Jonathan Burke,§ James F. Parsons,|| Richard N. Armstrong,‡ and Heini W. Dirr*,§

Departments of Biochemistry and Chemistry, Center in Molecular Toxicology, Vanderbilt University School of Medicine, Nashville, Tennessee 37232-0146, Protein Structure-Function Research Unit, School of Molecular and Cell Biology, University of the Witwatersrand, Johannesburg 2050, South Africa, and Center for Advanced Research in Biotechnology of the Maryland Biotechnology Institute and the National Institutes of Standards and Technology, Guldelsky Drive, Rockville, Maryland 20850

Received September 27, 2005; Revised Manuscript Received December 14, 2005

ABSTRACT: Canonical glutathione (GSH) transferases are dimeric proteins with subunits composed of an N-terminal GSH binding region (domain 1) and a C-terminal helical region (domain 2). The stabilities of several GSH transferase dimers are dependent upon two groups of interactions between domains 1 and 2 of opposing subunits: a hydrophobic ball-and-socket motif and a buried charge cluster motif. In rGSTM1-1, these motifs involve residues F56 and R81, respectively. The structural basis for the effects of mutating F56 to different residues on dimer stability and function has been reported (Codreanu et al. (2005) *Biochemistry 44*, 10605−10612). Here, we show that the simultaneous disruption of both motifs in the F56S/R81A mutant causes complete dissociation of the dimer to a monomeric protein on the basis of gel filtration chromatography and multiple-angle laser light scattering. The fluorescence and far-UV CD properties of the double mutant as well as the kinetics of amide H/D exchange along the polypeptide backbone suggest that the monomer has a globular structure that is similar to a single subunit in the native protein. However, the mutant monomer has severely impaired catalytic activity, suggesting that the dimer interface is vital for efficient catalysis. Backbone amide H/D exchange kinetics in the F56S and F56S/R81A mutants indicate that a reorganization of the loop structure between helix α2 and strand *β*3 near the active site is responsible for the decreased catalytic activity of the monomer. In addition, the junction between the α4 and α5 helices in F56S/R81R shows decreased H/D exchange, indicating another structural change that may affect catalysis. Although the native subunit interface is important for dimer stability, urea-induced unfolding of the F56S/R81A mutant suggests that the interface is not essential for the thermodynamic stability of individual subunits. The H/D exchange data reveal a possible molecular basis for the folding cooperativity observed between domains 1 and 2.

Protein interfaces are generally defined in terms of their physical and chemical properties (*1*); however, the mechanisms of subunit recognition are only partly understood (*2*−*4*). The GSH[1] transferases and related proteins are multifunctional enzymes with variable oligomeric structures. The canonical GSH transferases are typically dimers, while structurally related proteins such as glutaredoxin 2 and the chloride intracellular channel are monomers (*5*, *6*). The canonical GSH transferases are separated into various classes (α, *μ*, *π*, *σ*, *θ*, *ζ*, and *ω*) depending on sequence and structure (*7*). Despite the fact that GSH transferase subunits from different classes are structurally similar, molecular recognition at the dimer interface is highly specific. In vivo, only subunits from within the same class (e.g., *μ*) associate to form homodimers (e.g., M1-1, M2-2) and heterodimers (e.g., M1-2).

The structure of each subunit is composed of an N-terminal GSH binding domain (domain 1) and a C-terminal all-helical domain (domain 2). The key structural elements from both domains form the dimer interface, as illustrated in Figure 1 for the *μ* class rGSTM1-1. Two groups of interactions form the core of the interface contacts. The first is a hydrophobic ball-and-socket motif between F56 located on a loop (56-loop) in domain 1 and a group of hydrophobic side chains

† Supported by the University of the Witwatersrand, the South African Foundation for Research and Development Grant 2053559, Wellcome Trust Grant 060799, Forgarty International Research Collaboration Award R03 TW00779, and Grants R01 GM30910, P30 ES00267, and T32 ES07028 from the National Institutes of Health.

* To whom correspondence should be addressed. E-mail: heinid@gecko.biol.wits.ac.za. Fax: +27 11 7176351. Tel: +27 11 7176352.

‡ Vanderbilt University School of Medicine.

§ University of the Witwatersrand.

|| Center for Advance Research in Biotechnology of the Maryland Biotechnology Institute and the National Institutes of Standards and Technology.

[1] Abbreviations: rGSTM1-1, rat glutathione transferase class Mu isozyme 1-1; GSH, glutathione; GSO_3^-, glutathione sulfonate; DTNB, dithiobis(2-nitrobenzoic acid); ANS, 8-aniline-1-naphthalenesulfonate; CDNB, 1-chloro-2,4-dinitrobenzene; PCR, polymerase chain reaction; IPTG, isopropyl-*β*-D-thiogalactopyranoside; MOPS, 3-(*N*-morpholino)-propanesulfonic acid; OD, optical density; LB, Luria broth; Tris, tris-(hydroxymethyl)aminomethane; EDTA, ethylenediaminedtetraacetic acid; DTT, dithiothreitol; SDS-PAGE, sodium dodecyl sulfate polyacrylamide gel electrophoresis; MW, molecular weight; ESI-MS, electrospray ionization mass spectrometry; UV, ultraviolet; CD, circular dichroism; SEC-HPLC, size exclusion chromatography−high-pressure liquid chromatography.

10.1021/bi0519506 CCC: $33.50
Published on Web 01/25/2006

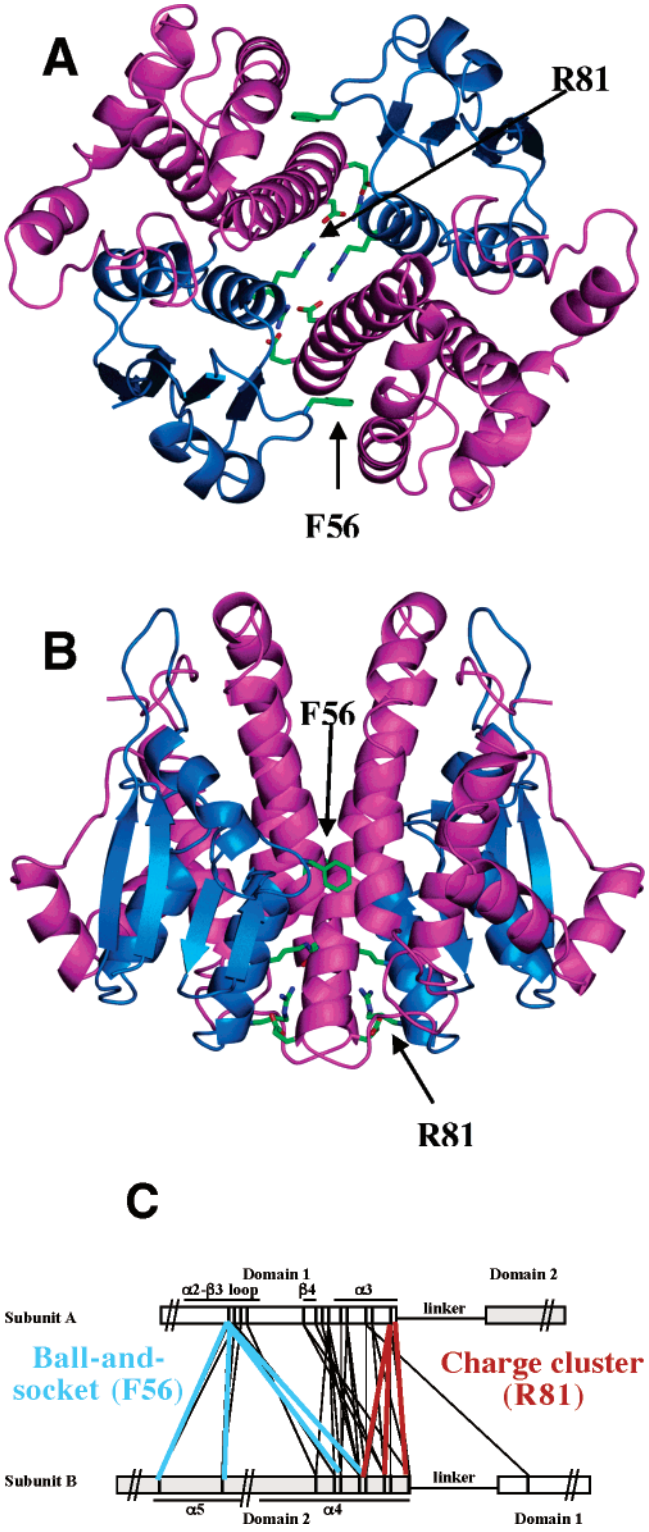

FIGURE 1: Primary interactions across the dimer interface of rGSTM1-1. (A and B) Ribbon diagrams of the protein backbone: domain 1 (the thioredoxin fold) is colored blue, and domain 2 (the helical domain) is colored magenta. The side chains shown are representative of the hydrophobic "ball-and-socket" motif (F56 "the ball") as well as the charge cluster (R81). (C) All of the intersubunit interactions, with those in cyan for the "ball-and-socket" motif and those in red for the charge cluster.

on the α4 and α5 helices of domain 2 (Figure 1). The second is a cluster of electrostatic interactions between β4/α3 of domain 1 and α4 of domain 2. These interactions include a salt link between R81 of domain 1 and E90/D97 of domain 2 (Figure 1).

Both interaction motifs appear to be important for dimer stability in GSH transferases with similar interface structures. Previously, we have shown that interruption of the ball-and-socket motif (F56S) in rGSTM1-1 increased the K_d value of the dimer 42-fold to 0.5 μM relative to the native enzyme (*8*). Individual disruption of both motifs (F52A and R69E, respectively) in the rGSTA1-1 isoenzyme, as well as the combined mutations, results in a shift in the equilibrium from dimer toward monomer in sedimentation assays (*9*).

The stability and functionality of the individual subunits in the absence of the dimer interface are unknown. Glutaredoxin 2 is structurally similar to a canonical GSH transferase monomer (*6*) and is considered to be a possible evolutionary precursor to this family of GSH transferases (*10*). This idea suggests that the intersubunit interactions in the canonical GSH transferases may not be essential for the thermodynamic stability of the monomer.

In the present study, we have disrupted both subunit interface motifs in the rGSTM1-1 enzyme in order to gain a further insight into the nature and mechanisms of subunit recognition in GSH transferases and to evaluate the stability and functionality of the individual subunits. Unlike the F56S mutant that forms dimers at the protein concentrations used in previous studies (*8*), the double mutant F56S/R81A yields only the monomeric form of rGSTM1-1. The influence of the dimer interface on GSH transferase, structure, stability, and function are reported in this paper.

EXPERIMENTAL PROCEDURES

Chemicals. GSH was obtained from ICE Biomedical Inc. (Aurora, OH). TFE (99+% grade), ANS, GSO_3^-, and CDNB were purchased from Sigma-Aldrich (St. Louis, MO). All other reagents were of analytical grade.

Preparation of the F56S/R81A Mutant Protein. The expression vectors for the F56S/R81A mutant of M1-1 were generated by site-specific mutagenesis as previously described (*8*). The codon CGC (R) in the pET20b vector of the F56S mutant was switched to GCC (A) via PCR amplification with primers containing the desired mutation. The R81A mutation was confirmed by submission to the Vanderbilt Sequencing Core. The mutant enzyme was overexpressed in *E. coli* strain BL21(DE3) Tuner. The cell culture was grown at 30 °C in LB media with ampicillin (100 mg/mL), with vigorous shaking until the OD_{600} value was 1.0. Cells were cooled to 15 °C and then induced with IPTG for 16 h (0.1 mM final concentration). Cells were then harvested by centrifugation (7000*g*, 30 min, 4 °C) and pellets resuspended in 20 mM Tris buffer (pH 6.8). Cells were treated with lysozyme for 30 min, lysed by sonication, and treated with 1 mL of 10X protease inhibitor cocktail solution, and then cell debris was removed by centrifugation (15 000*g*, 60 min, 4 °C). The supernatant was then treated with benzonase for 1 h at room temperature to digest nucleic acids and then dialyzed against 20 mM MOPS buffer containing 1 mM EDTA and DTT (pH 6.8). The proteins were applied to a cationic exchange SP-Sepharose column (2 × 15 cm), previously equilibrated with the same buffer and eluted with linear salt gradient (0−300 mM NaCl) in the same buffer. Fractions containing protein were pooled together and dialyzed against 20 mM KH_2PO_4 buffer containing 1 mM DTT (pH 6.8). The protein solutions were further applied to

a hydroxyapatite column (2 × 10 cm), previously equilibrated with the phosphate buffer, and eluted with a buffer gradient (20−400 mM KH_2PO_4) containing 1 mM DTT (pH 6.8). Fractions containing protein were pooled together and dialyzed against 100 mM KH_2PO_4 buffer (pH 7.0). The protein was then loaded onto a 120 mL Sephacryl S-100 gel filtration column that was preequilibrated with the same buffer. Peaks containing protein were pooled together. The purity of the protein was confirmed by visual inspection of a Commassie stained SDS-PAGE, and the mass was confirmed by ESI-MS. Protein concentration was measured using a molar extinction coefficient of 40 060 M^{-1} cm^{-1} (*11*). Protein was concentrated to 600 μM and then separated into 125 mL aliquots. Individual aliquots were flash frozen on dry ice and stored at −80 °C. Samples were thawed on ice and used the same day.

Size Exclusion Chromatography. The hydrodynamic behavior of the native and F56S/R81A proteins was first characterized by size exclusion chromatography through a Pharmacia LKB 2150 HPLC system with a JASCO FP-2020 Plus fluorescence detector and a Tosohaas TSKGEL G2000SWXL column (7.8 mm × 300 mm). Samples (20 μL) of the protein at concentrations ranging between 0.5 and 600 μM were injected and eluted at 20 °C with 0.1 M KH_2PO_4, 0.1 M Na_2SO_4, 0.05% NaN_3 (pH 6.7) buffer at a flow rate of 0.5 mL/min. The elution of the protein was monitored continuously by the intrinsic protein fluorescence with excitation and emission wavelengths of 295 and 340 nm, respectively.

Molecular Mass from Multiangle Laser Light Scattering. The solution molecular masses of the native GSH transferase (rGSTM1-1) and its double mutant (F56S/R81A) were determined by multiangle laser light scattering and interferometric refractometry. Samples were subjected to gel filtration chromatography (Shodex KW-802.5; 8 mm × 300 mm; 0.5 mL/min) in 50 mM HEPES, 100 mM NaCl, 0.1 mM EDTA buffer (pH 7.5) prior to in-line analysis with a DAWN EOS multiangle light scattering detector, an Optilab DSP refractive index detector, and an Agilent 1000 UV detector. All samples were filtered with a 0.2 μm filter just prior to analysis. The injection volume was 20 μL. Stock protein solutions were 600 μM (mutant) or 770 μM (native). Molecular masses were calculated with the ASTRA software package (*12*).

Spectroscopic Methods. Spectroscopic measurements were made at 20 °C. CD and fluorescence measurements were made with a JASCO Model 810 CD spectropolarimeter and a Hitachi Model 850 fluorescence spectrometer, respectively. Tryptophan fluorescence was monitored at an excitation wavelength of 295 nm, and the binding of the anionic dye, ANS, to protein was monitored by fluorescence enhancement using an excitation wavelength of 390 nm.

Enzyme Activity. Enzyme activity was assayed spectrophotometrically at 340 nm by monitoring the conjugation reaction between GSH and CDNB (*13*). All kinetic experiments were carried out in 0.1 M KH_2PO_4 buffer (pH 6.5) and 25 °C with 500 nM enzyme. The final concentration of CDNB was 1.0 mM, while that of GSH was 10−40 mM. All rates are corrected for the background reaction.

GSO_3^- Binding. A 2 μM solution of F56S/R81A in 20 mM NaH_2PO_4 buffer (pH 7.0) was titrated with a 600 mM solution of GSO_3^- and the fluorescence intensity at 341 nm (excitation at 295 nm) measured. The fluorescence quenching data, corrected for dilution, were fitted by nonlinear least-squares regression using the program SigmaPlot 8 (SPSS Inc.).

Hydrogen Deuterium Exchange. H/D exchange experiments were designed similarly to those reported previously (*14*). Deuterium exchange was initiated by diluting 10 μL of the equilibrated protein solution (600 μM) 10-fold with 90 μL of D_2O. The protein/D_2O solution was incubated at 25 °C for various times (from 15 s to 8 h). At each time point, the reaction was quenched by cooling (tubes transferred to an ice bath) and acidified by adding 100 μL of quench buffer (0.1 M KH_2PO_4, (pH 2.4) in H_2O at 0 °C). After 30 s, 5 μL of pepsin (15 mg/mL in H_2O at 0 °C) was added to the quenched sample and incubated on ice for 5 min. All of the samples for one protein (15 time points) were prepared individually and run on the same day.

Electrospray Ionization Mass Spectrometry. The extent of deuterium incorporation into the peptide fragments was determined by LC/MS using the same protocol described previously (*14*). Mass determinations were measured on a Finnigan TSQ Quantum triple-quadrupole mass spectrometer (Finnigan Corp., San Jose, CA), both equipped with a standard electrospray ionization source outfitted with a 100 μm i.d. deactivated fused silica capillary. The mass spectrometer was operated in full scan mode using Quad 1. The analyzer was calibrated and tuned to unit resolution with a peak width at half-height of 0.7. The data were collected from *m*/*z* 300 to 900 with a 1 s scan time. Data acquisition and spectral analysis were conducted using Finnigan Xcalibur software (version 1.3) on a Dell Optiplex GX270 computer running the Microsoft Windows 2000 operating system. The centroid data were analyzed using MagTran 1.0 beta9 software written by Zhang and Marshall (*15*).

Kinetic Analysis of H/D Exchange. The amount of deuterium incorporated in each peptide was adjusted for back-exchange as described previously (*14*) and plotted versus time. Progress curves for individual peptides were fitted to the sum of first-order rate terms according to eq 1,

$$D = N - \sum_{i=1}^{N} \exp(-k_i t) \quad (1)$$

using the program Prism 4.0 (Graphpad Software), where D is the deuterium content of a peptide, N is the number of peptide amide protons, k_i is the exchange rate constant for each amide hydrogen, and t is the time allowed for isotope exchange (*16*).

Urea-Induced Unfolding. All unfolding experiments were performed at 20 °C in 20 mM NaH_2PO_4 buffer containing 0.1 M NaCl, 1 mM EDTA, and 0.02% NaN_3 (pH 6.5) as described previously (*17*). Protein and urea concentrations were 2 μM and 0−8 M, respectively. Tryptophan fluorescence (excitation at 295 nm; emission at 341 and 355 nm for the folded and unfolded protein, respectively) and far-UV CD ellipticities at 222 nm were used to monitor structural changes. Equilibrium unfolding data were fitted by nonlinear least-squares regression as described previously (*17*).

RESULTS

Global Structural Properties. Gel filtration experiments with the F56S/R81A mutant indicate that the protein elutes

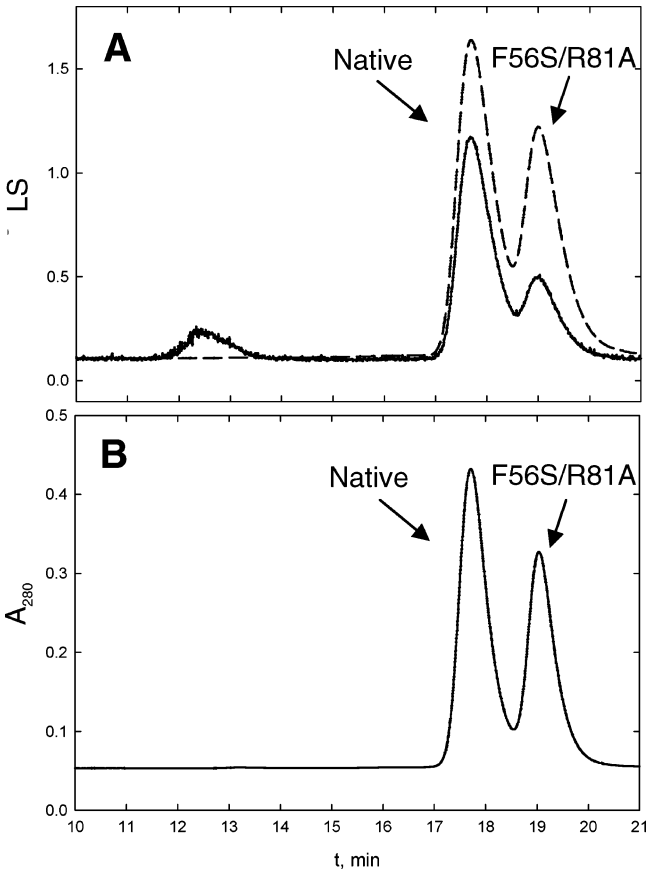

FIGURE 2: Chromatograms of (A) the output signal from the DAWN light scattering detector (solid line) and the concentration trace from the refractometer (dashed line) and (B) the output from the UV detector (280 nm). The signal at 12.5 min from the 90° light-scattering channel (A) represents a small amount of protein aggregate found in both samples. The molecular mass moments from the multiangle laser light scattering analysis were 26 100 ± 300 g/mol for the F56S/R81A mutant and 50 800 ± 200 g/mol for the native enzyme.

as a single species at concentrations ranging from 0.2 to 600 μM (data not shown). The elution volume on a calibrated Tosohaas TSKGEL G2000SWXL column (7.8 mm × 300 mm) corresponds to the expected size of 26 kDa for a folded monomer. This initial observation was confirmed by combining gel filtration chromatography coupled with multiangle laser light scattering (see Experimental Procedures) of both the native and mutant proteins. These analyses show that the F56S/R81A mutant is a single species with a molecular mass moment of 25 400 ± 200 g/mol, consistent with the protein being a monomer. As expected, the native enzyme behaves as a single species with a mass of 51 500 ± 200 g/mol. When a mixture of the two proteins was analyzed, the native enzyme and the F56S/R81A mutant were well resolved (Figure 2), and return molecular masses were consistent with those from analysis of the individual samples (Figure 2, legend).

Far- and near-UV CD and tryptophan fluorescence spectroscopy indicate that the double mutant has a secondary structure that is nativelike. Small perturbations in the environments of the tryptophan residues in the mutant are evident from the far-UV portion of the CD spectra and the fluorescence emission spectra (data not shown). The spectra of F56R/R81A resemble those of the F56S mutant of rGSTM1-1 (*8*) and the related isoenzyme rGSTM2−2 (*17*).

Table 1: Efficiency of CDNB Conjugation in the Native and Dimer Interface Mutants

enzyme	k_{cat} (s^{-1})	K_m^{GSH} (mM)	k_{cat}/K_m^{GSH} ($M^{-1}\,s^{-1}$)
native[a]	18 ± 2	0.036 ± 0.004	(5.0 ± 0.8) × 10^5
F56S[b]	90 ± 10	20 ± 2	(4.5 ± 0.7) × 10^3
F56S/R81A	≫0.2	≫40	5.2 ± 0.4

[a] Data from ref (*18*). [b] Data from ref (*8*).

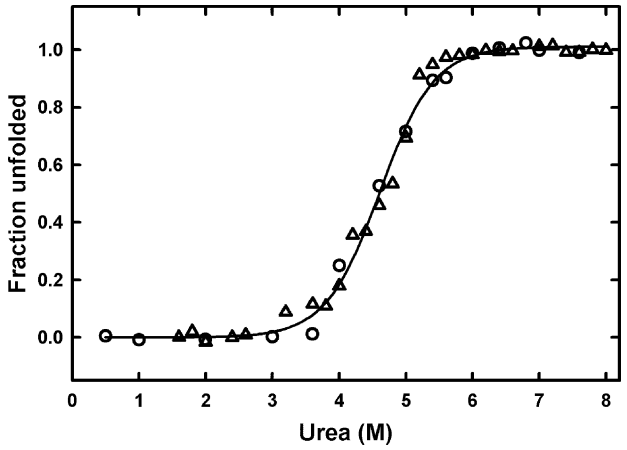

FIGURE 3: Unfolding curves of the F56S/R81A mutant: (circles) fluorescence; and (triangles) CD ellipticity at 222 nm. The solid line represents a nonlinear least-squares regression fit to the data according to a two-state model with folded and unfolded monomers (*16*).

Functional Properties of F56S/R81A rGSTM1. The binding affinity of GSO_3^- for F56S/R81A was determined by fluorescence titration (K_d = 24 mM). The affinity is substantially less than that for the native dimer (K_d = 2.8 μM) and indicates a loss of about 9.2 kcal/mol in binding energy for the monomeric protein. Unlike the F56S mutant, which shows saturation kinetics and can achieve or exceed wild-type-like activity at saturating GSH (*8*), the reaction velocity of the F56S/R81A mutant exhibited a linear concentration dependence up 40 mM GSH. The k_{cat}/K_M^{GSH} for the double mutant is reduced by a factor of 10^5 compared to that of the native enzyme (*18*) (Table 1). The K_M for GSH is ≫40 mM.

ANS Binding. The location of the binding site for ANS in the mutant proteins F56S and F56S/R81A is unknown, but the dye has been shown to bind to many GSH transferases at the active site (*19*) and/or along the dimer interface (*20*, *21*), making the fluorescent dye a useful probe for monitoring intersubunit and intrasubunit structural alterations (*8*, *17*, *19*). The spectral properties of ANS bound to F56S/R81A differ from those of the native enzyme (data not shown) but are similar to those for the dye bound to the F56S mutant (*8*). This result suggests that the dye-binding site in the double mutant is affected primarily by the loss of the ball-and-socket motif and not by disruption of the dimeric structure and provides further evidence that the loss of the dimer interface does not substantially destabilize the individual subunits.

Equilibrium Unfolding of F56S/R81A rGSTM1. Like native rGSTM1-1 and its F56S variant, the monomeric F56S/R81A mutant unfolds reversibly. Urea-induced unfolding of F56S/R81A, monitored by far-UV CD and tryptophan fluorescence, is shown in Figure 3. Both probes yield overlapping transitions indicating a two-state unfolding process with the simultaneous loss of secondary and tertiary structures. The

Table 2: Data from Equilibrium Unfolding of the Native M1-1, F56S, and F56S/R81A Mutants[a]

rGST M1-1	model	C_m (M urea)	$\Delta G(H_2O)$ (kcal/mol)	m (kcal/(mol/M urea))
native	$N_2 \leftrightarrow 2I$	3.1	10.8	1.0
	$I \leftrightarrow U$	5.2	16.5	3.5
F56S	$N_2 \leftrightarrow 2I$	2.3	10.3	1.0
	$I \leftrightarrow U$	5.1	15.9	3.1
F56S/R81A	$I \leftrightarrow U$	4.6	10.1	2.0 (2.5)[b]

[a] Data for wild-type and F56S taken from refs (*16*) and (*10*), respectively. [b] Value calculated according to ref (*22*).

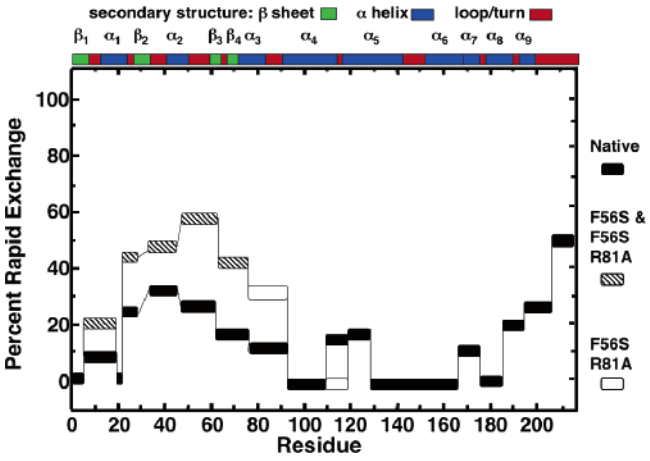

FIGURE 4: Amide protons exchanged by the first 15 s for peptides from native, F56S (*23*), and F56S/R81A rGSTM1-1. Deviations of F56S and F56S/R81A from the native are shown as hashed boxes. Deviations of F56S/R81A from both native and F56S are shown as open boxes.

monomeric mutant does not appear to sample high-energy, partially unfolded states under native (0−3 M urea) and denaturing (>3 M urea) conditions. In contrast, the native enzyme and F56S mutant unfold via a three-state process ($N \leftrightarrow 2I \leftrightarrow 2U$) with the dimer−monomer equilibrium shifted toward the monomeric intermediate, I, for the F56S mutant (*17*) (see Table 2). The lower C_m and ΔG (H_2O) values for F56S/R81A, in comparison to those for the $I \leftrightarrow U$ transitions of native enzyme and the F56S mutant (Table 2), indicate a reduced stability of the monomeric mutant. Furthermore, the lower experimental m value as compared to that predicted for the double mutant (Table 2) indicates that its unfolding is less cooperative and that less surface area becomes exposed to solvent upon unfolding.

Amide H/D Exchange and Structural Dynamics. Pepsin digestion yields 42 well-resolved peptides that are common to the native, F56S, and F56S/R81A proteins representing coverage of 97% of the sequence (Figure 4). The two regions not covered are residues 28−33 and residues 47−48. The profile of rapidly exchanging amide protons for selected peptides from native, F56S (*23*), and F56S/R81A are shown in Figure 4. The kinetic profile of the F56S/R81A mutant resembles that for the native and F56S proteins, indicating that the combined F56S and R81A mutations do not induce major changes in the core structure of the monomeric protein, a result consistent with the structural data presented above.

Although the H/D exchange kinetics of the F56S and F56S/R81A mutants are similar, they do exhibit interesting differences. For example, in comparison to F56S, the F56S/R81A mutant shows enhanced H/D exchange kinetics for peptides 75−91 and 92−96 but reduced rates of exchange for peptide 110−119, as illustrated in Figures 4 and 5 and listed in Table 3. Peptides 92−96 and 75−91 (which contains the R81A mutation) are located at the core of the charge cluster. These two peptides are primarily involved in intersubunit interactions and would be expected to show increases in H/D exchange kinetics upon loss of the dimeric structure. The decrease in solvent accessibility of peptide 110−119 is most likely due to the reorganization of the junction between helices α4 and α5 (Figure 5A). Reorganization of this junction is not unexpected, because these helices are involved in many of the intersubunit interactions (Figure 1C). The loss of solvent accessibility indicates that the junction and the α4 and α5 helices form a tighter interaction or are folded in toward the core of the monomer structure. The α4 and α5 helices are part of a channel that controls access to the active site in the native enzyme (*14*). The alternate conformation of the junction, reflected in the decreased amide H/D exchange, may contribute to the reduced catalytic activity observed in the double mutant.

The lack of an increase in amide H/D exchange in peptides 19−21 in helix α1, 97−100 in helix α4, and 158−163 in helix α6 (Figures 4 and 6) demonstrates that the conformation and stability of these regions are preserved after dissociation of the dimer to form the F56S/R81A monomer. Peptide 97−100 is involved in intersubunit interactions and become exposed to solvent upon disruption of the dimer yet shows no increase in exchange. This could result from a close interaction with peptide 158−163 (Figure 6) and may indicate an important structural motif for the stability of domain 2. Peptide 158−163 is also in close proximity to peptide 19−21. The absence of increases in exchange for either of these peptides in the monomeric F56S/R81A mutant may indicate an important interdomain interaction.

DISCUSSION

Properties of a Stable Monomer. We have previously shown that wild-type rGSTM1-1 undergoes a reversible dissociation of its subunits with an approximate K_d value of 0.012 μM. Disruption of the ball-and-socket motif, with the introduction of the F56S mutation, shifts the equilibrium toward the monomeric species (K_d of 0.5 μM) (*8*). In the present study, the intersubunit charge cluster motif was disrupted with the R81A mutation. This site was chosen because it is the only residue in the cluster that directly participates in an intersubunit interaction. While mutations at either the ball-and-socket motif or the charge cluster motif have been shown to produce equilibrium mixtures of dimeric and monomeric forms of GSH transferases (*8*, *9*), this study demonstrates that the simultaneous introduction of single mutations in both motifs is sufficient to generate a monomeric enzyme with a compact folded structure, albeit with greatly reduced catalytic activity.

Dimer-Dependent Enzyme Activity. The binding of GSH or the inhibitor GSO_3^- to the F56S mutant of rGSTM1-1 restores a more nativelike conformation in the active site (*8*). At sufficiently high GSH concentrations the F56S mutant exhibits robust catalytic activity (*8*, *23*). The F56S mutant does not have the fully functional hydrophobic ball-and-socket motif required to stabilize the 56-loop between α2 and β3 near the active site. In fact, residues in the 56-loop

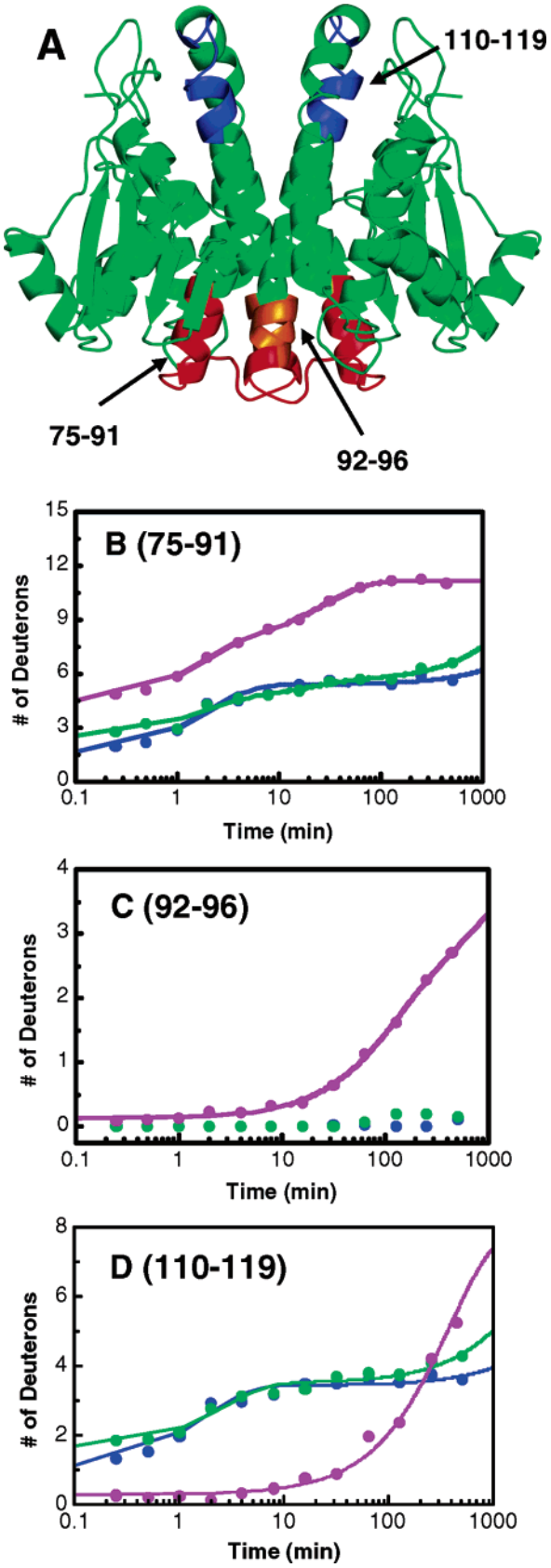

FIGURE 5: Peptides in F56S/R81A with exchange behavior that differs from that of F56S. (A) Ribbon diagram of the rGSTM1-1 backbone (green) showing increases in fast phase exchange (red), increases in slow phase exchange (orange), and decreases in exchange (blue). (B−D) Kinetics of amide H/D exchange for the three peptides 75−91 (B), 92−96 (C) and 110−119 (D). The kinetic profiles for the native enzyme, the F56S mutant (*23*), and the F56S/R81A mutant are shown in blue, green, and magenta, respectively.

Table 3: Rate Constants and Amplitudes for Main-Chain Amide H/D Exchange into F56S/R81A of Peptides 75−91, 92−96, and 110−119 (Figure 5)

peptide	A_1 (D)	k_1 (min^{-1})	A_2 (D)	k_2 (min^{-1})
75−91	3.1 ± 0.3	0.6 ± 0.2	3.6 ± 0.3	0.042 ± 0.006
92−96	1.8 ± 0.5	0.009 ± 0.002	2.1 ± 0.5	0.001 ± 0.0005
110−119	7.7 ± 0.1	0.003 ± 0.0001		

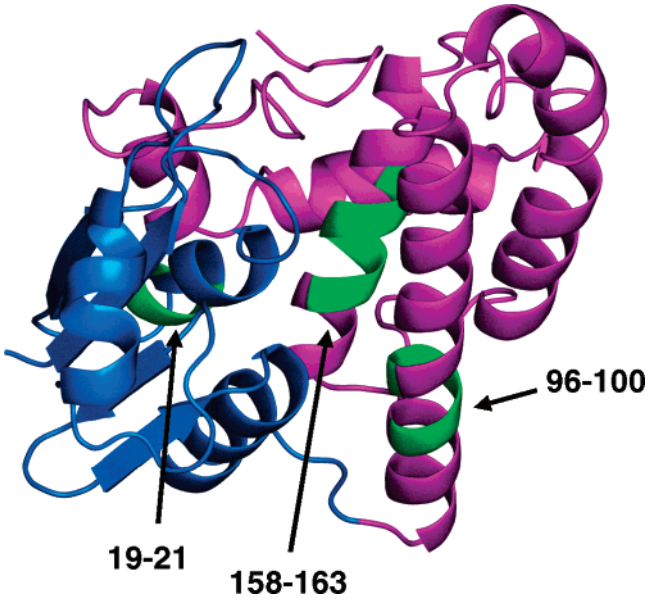

FIGURE 6: Ribbon diagram of one subunit of rGSTM1-1: domain 1 (blue) and domain 2 (magenta). F56S/R81A peptides that show no H/D exchange during the length of the experiment are shown in green: 19−21, 97−100, and 158−163. Native and F56S also show no H/D exchange into these peptides during the length of the experiment.

are in contact with Y6 in the active site, a residue that is crucial for efficient catalysis. Although the backbone of the 56-loop appears to have similar H/D exchange characteristics in the F56S and F56S/R81A mutants (Figure 4), nativelike activity cannot be achieved in the monomer (Table 1). These facts suggest that the dimer interface helps enforce the conformation of the loop that is vital for GSH binding and efficient catalysis.

The disruption of the 56-loop and the ability to bind GSH in a productive manner is probably the principal reason for the reduced catalytic efficiency of the F56S and F56S/R81A mutants. However, the H/D exchange results do indicate a change in structure and dynamics at the junction between the α4 and α5 helices (peptide 110−119). This region contains Y115, a residue that is located atop a channel that is important for substrate access and product release in the dimer (*14*). The reduced H/D exchange suggests a tighter interaction between the two helices or with the rest of the monomer. At this point it is unclear whether the change in structure and dynamics of this region contributes to the further impairment of the catalytic efficiency of the monomer.

Cooperative Unfolding. The tertiary structure of the F56S/R81A mutant enzyme is more loosely packed than that of either the native enzyme or F56S mutant. However, the double mutation does not significantly impact the intrasubunit interactions between domains 1 and 2, as suggested by the similarity in the H/D exchange kinetics. Nevertheless, the

equilibrium unfolding data for the double mutant demonstrates that intersubunit interactions make significant contributions to stabilizing the tertiary structures of subunits in GSH transferase dimers as in the native and F56S proteins. These interactions are not obligatory for the stabilizing interaction of domains 1 and 2 in each subunit. At equilibrium, domains 1 and 2 do not unfold independently but unfold in a concerted manner.

Molecular Basis for Domain Cooperativity. A concerted unfolding model for the monomeric double mutant suggests interdomain cooperativity. The strongest evidence for an interdomain interaction comes from the H/D exchange behavior of peptides 19−21, 97−100, and 158−163 (Figure 6). These peptides show no amide H/D exchange during the time course of the experiment, a fact that indicates a very stable monomeric fold and not a molten globule-like state. The fact that these protein regions are in close proximity to each other and cross the domain barrier (domain 1 (19−21) and domain 2 (158−163)) could indicate a stable core of interactions between domains 1 and 2 that constitute the cooperative link.

The stability of individual GSH transferase subunits in the absence of the dimer interface suggests that the evolution of intersubunit interactions has arisen more recently than evolution of the monomer itself. This is consistent with the hypothesis that the canonical GSH transferases arose from enzymes similar to glutaredoxin 2 (*10*). It also suggests that the selectivity of intersubunit interactions for isoenzymes of a particular class arose to fine-tune the enzyme structure to broaden substrate specificity and biological function.

SUPPORTING INFORMATION AVAILABLE

Table S1, containing a complete set of the rate constants and amplitudes used to fit kinetic profiles for all peptides, and Figures S1−S42, describing the kinetic profiles for H/D exchange for all peptides. This material is available free of charge via the Internet at http://pubs.acs.org.

REFERENCES

1. Jones, S., and Thornton, J. M. (1995) Protein−protein interactions: a review of protein dimer structures, *Prog. Biophys. Mol. Biol. 63*, 31−65.
2. Keskin, O., Tsai, C. J., Wolfson, H., and Nussinov, R. (2004) A new, structurally nonredundant, diverse data set of protein−protein interfaces and its implications, *Protein Sci. 13*, 1043−1055.
3. Keskin, O., and Nussinov, R. (2005) Favorable scaffolds: proteins with different sequence, structure and function may associate in similar ways, *Protein Eng. Des. Sel. 18*, 11−24.
4. Keskin, O., Ma, B., and Nussinov, R. (2005) Hot regions in protein-protein interactions: the organization and contribution of structurally conserved hot spot residues, *J. Mol. Biol. 345*, 1281-1294.
5. Harrop, S. J., DeMaere, M. Z., Fairlie, W. D., Reztsova, T., Valenzuela, S. M., Mazzanti, M., Tonini, R., Qiu, M. R., Jankova, L., Warton, K., Bauskin, A. R., Wu, W. M., Pankhurst, S., Campbell, T. J., Breit, S. N., and Curmi, P. M. (2001) Crystal structure of a soluble form of the intracellular chloride ion channel CLIC1 (NCC27) at 1.4-A resolution, *J. Biol. Chem. 276*, 44993−45000.
6. Xia, B., Vlamis-Gardikas, A., Holmgren, A., Wright, P. E., and Dyson, H. J. (2001) Solution structure of *Escherichia coli* glutaredoxin-2 shows similarity to mammalian glutathione-Stransferases, *J. Mol. Biol. 310*, 907−918.
7. Sheehan, D., Meade, G., Foley, V. M., and Dowd, C. A. (2001) Structure, function and evolution of glutathione transferases: implications for classification of nonmammalian members of an ancient enzyme superfamily, *Biochem. J. 360*, 1−16.
8. Hornby, J. A., Codreanu, S. G., Armstrong, R. N., and Dirr, H. W. (2002) Molecular recognition at the dimer interface of a class mu glutathione transferase: role of a hydrophobic interaction motif in dimer stability and protein function, *Biochemistry 41*, 14238−14247.
9. Vargo, M. A., Nguyen, L., and Colman, R. F. (2004) Subunit interface residues of glutathione S-transferase A1-1 that are important in the monomer−dimer equilibrium, *Biochemistry 43*, 3327−3335.
10. Ladner, J. E., Parsons, J. F., Rife, C. L., Gilliland, G. L., and Armstrong, R. N. (2004) Parallel evolutionary pathways for glutathione transferases: structure and mechanism of the mitochondrial class kappa enzyme rGSTK1-1, *Biochemistry 43*, 352−361.
11. Edelhoch, H. (1967) Spectroscopic determination of tryptophan and tyrosine in proteins, *Biochemistry 6*, 1948−1954.
12. Wyatt, J. P. (1993) Light scattering and the absolute characterization of macromolecules, *Anal. Chim. Acta 272*, 1−40.
13. Habig, W. H., and Jakoby, W. B. (1981) Assays for Differentiation of Glutathione-Stransferases, *Methods Enzymol. 77*, 398−405.
14. Codreanu, S. G., Ladner, J. E., Xiao, G., Stourman, N. V., Hachey, D. L., Gilliland, G. L., and Armstrong, R. N. (2002) Local protein dynamics and catalysis: detection of segmental motion associated with rate-limiting product release by a glutathione transferase, *Biochemistry 41*, 15161−15172.
15. Zhang, Z., and Marshall, A. G. (1998) A universal algorithm for fast and automated charge state deconvolution of electrospray mass-to-charge ratio spectra, *J. Am. Soc. Mass Spectrom. 9*, 225−233.
16. Zhang, Z., Post, C. B., and Smith, D. L. (1996) Amide hydrogen exchange determined by mass spectrometry: application to rabbit muscle aldolase, *Biochemistry 35*, 779−791.
17. Hornby, J. A., Luo, J. K., Stevens, J. M., Wallace, L. A., Kaplan, W., Armstrong, R. N., and Dirr, H. W. (2000) Equilibrium folding of dimeric class mu glutathione transferases involves a stable monomeric intermediate, *Biochemistry 39*, 12336−12344.
18. Parsons, J. F., Xiao, G., Gilliland, G. L., and Armstrong, R. N. (1998) Enzymes harboring unnatural amino acids: mechanistic and structural analysis of the enhanced catalytic activity of a glutathione transferase containing 5-fluorotryptophan, *Biochemistry 37*, 6286−6294.
19. Dirr, H. W., Little, T., Kuhnert, D. C., and Sayed, Y. (2005) A conserved N-capping motif contributes significantly to the stabilization and dynamics of the C-terminal region of class alpha glutathione S-transferases, *J. Biol. Chem. 280*, 19480−19487.
20. Stevens, J. M., Hornby, J. A., Armstrong, R. N., and Dirr, H. W. (1998) Class sigma glutathione transferase unfolds via a dimeric and a monomeric intermediate: impact of subunit interface on conformational stability in the superfamily, *Biochemistry 37*, 15534−15541.
21. Sluis-Cremer, N., Naidoo, N. N., Kaplan, W. H., Manoharan, T. H., Fahl, W. E., and Dirr, H. W. (1996) Determination of a binding site for a nonsubstrate ligand in mammalian cytosolic glutathione S-transferases by means of fluorescence-resonance energy transfer, *Eur. J. Biochem. 241*, 484−488.
22. Myers, J. K., Pace, C. N., and Scholtz, J. M. (1995) Denaturant *m* values and heat capacity changes: relation to changes in accessible surface areas of protein unfolding, *Protein Sci. 4*, 2138−2148.
23. Codreanu, S. G., Thompson, L. C., Hachey, D. L., Dirr, H. W., and Armstrong, R. N. (2005) Influence of the Dimer Interface on Glutathione Transferase Structure and Dynamics Revealed by Amide H/D Exchange Mass Spectrometry, *Biochemistry 44*, 10605−10612.

BI0519506